# $Ca^{2+}$ and cAMP open differentially dilating synaptic fusion pores

Dinara Bulgari[1], Samantha L. Cavolo[1+], Brigitte F. Schmidt[2], Katherine Buchan[2#], Marcel P. Bruchez[3*], David L. Deitcher[4], and Edwin S. Levitan[1,@]

[1]Department of Pharmacology and Chemical Biology, University of Pittsburgh, Pittsburgh, PA 15261 USA

[2]Department of Chemistry, Carnegie Mellon University, Pittsburgh, PA 15213 USA

[3]Departments of Chemistry, Department of Biology, and the Molecular Biosensor and Imaging Center, Carnegie Mellon University, Pittsburgh, PA 15213 USA

[4]Department of Neurobiology and Behavior, Cornell University, Ithaca, NY 14853 USA

[@]correspondence to elevitan@pitt.edu

current contact information: [+]Samantha.cavolo@AHN.org, [#]kb4162@nyu.edu

*deceased

The authors declare no competing interests.

25 pages, 6 figures

**ABSTRACT**

**Neuronal dense-core vesicles (DCVs) contain neuropeptides and much larger proteins that affect synaptic growth and plasticity. Rather than using full collapse exocytosis that is common in endocrine cells, DCVs at a native intact synapse, the *Drosophila* neuromuscular junction, release their contents via fusion pores formed by kiss and run exocytosis. Here fluorogen activating protein (FAP) imaging reveals the permeability range of synaptic DCV fusion pores and then shows that this constraint is circumvented by cAMP-induced extra fusions with dilating pores that result in DCV emptying. These $Ca^{2+}$-independent full fusions require PKA-R2, a PKA phosphorylation site on the fusion clamp protein complexin and the acute presynaptic function of Rugose/Neurobeachin, a PKA-R2 anchor implicated in learning and autism. Therefore, localized $Ca^{2+}$-independent cAMP signaling opens dilating fusion pores to release large cargo proteins that cannot pass through the narrower fusion pores that normally dominate spontaneous and $Ca^{2+}$-evoked synaptic protein release. Hence, two independent exocytosis triggers ($Ca^{2+}$ and cAMP) vary the composition of released proteins at the synapse by differentially adjusting DCV fusion pores.**

## INTRODUCTION

Neuronal dense-core vesicles (DCVs) contain a wide variety of secretory protein cargos including neuropeptides (with molecular weights of 0.6-30 kDa in *Drosophila*) and proteases that function in synaptic plasticity and growth (e.g., 70 kDa tissue plasminogen activator) (Huang *et al.*, 1996; Baranes *et al.*, 1998). Early studies of secretion from endocrine cells emphasized $Ca^{2+}$-induced DCV emptying by full collapse exocytosis that follows fusion pore dilation. However, studies of spontaneous and activity-evoked release by DCVs in the intact *Drosophila* neuromuscular junction (NMJ) with two different imaging approaches failed to detect DCV emptying and instead produced data consistent with release via fusion pores formed by kiss and run exocytosis (Wong *et al.*, 2015; Bulgari *et al.*, 2019). Partial release by kiss and run exocytosis of presynaptic DCVs is conducive with the cell biology of neurons: because these organelles are replaced by axonal transport that can take days, kiss and run exocytosis may prevent rapid depletion of stores at distal sites of release that are slow to refill. However, it is not known whether presynaptic fusion pores allow for release of large DCV cargos.

Imaging permeation through DCV fusion pores is difficult in native synapses that contain DCVs and small synaptic vesicles (SSVs) because fluid phase fluorophores used with endocrine cells (e.g., Takahashi *et al.*, 2002) cannot distinguish between the two vesicle types and cutting-edge superresolution microscopy methods that resolve fusion pore dilation rely on *in vitro* preparations (e.g., Anantharam *et al.*, 2011). Likewise, electrical and electrochemical fusion pore measurements (Sharma and Lindau, 2018) are not well suited to typical native cotransmitting synaptic boutons.

62 However, synaptic DCV fusion pores were detected recently using membrane-
63 impermeant malachite green (MG)-based fluorogens and a fluorogen activating protein
64 (FAP) targeted to the DCV lumen so that, upon opening of a fusion pore, fluorogens
65 pass through the fusion pore into the DCV to bind the FAP with picomolar affinity and
66 generate far-red fluorescence (Bulgari *et al.*, 2019). Because previously used
67 fluorogens varied in shape and constituent moieties, and their hydrodynamic sizes were
68 not characterized (Bulgari *et al.*, 2019), the permeability of presynaptic fusion pores was
69 not studied systematically. Nevertheless, an experimental approach for studying
70 synaptic fusion pore permeability was established.
71 Here a series of single chain PEGylated membrane impermeant MG fluorogens
72 and a FAP inserted into the neuropeptide *Drosophila* insulin-like peptide 2 (i.e., Dilp2-
73 FAP, Bulgari *et al.*, 2019) are used at the *Drosophila* NMJ to show that synaptic fusion
74 pores that open spontaneously and in response to activity are not permeable to large
75 DCV cargos. Then the conundrum of how such proteins can be efficiently released from
76 presynaptic DCVs is resolved by establishing that anchored, activated PKA acts via
77 complexin phosphorylation to open dilating fusion pores that results in DCV emptying.
78

79 **RESULTS**

80 *Synaptic DCV fusion pore permeability*

81 Fluorogens were synthesized via conjugating single chain polyethylene glycol
82 (PEG) adducts to MG. Their hydrodynamic sizes were then determined in comparison
83 to proteins by size exclusion fast protein liquid chromatography (FPLC) (see **Methods**).
84 The hydrodynamic properties of these fluorogens scaled with molecular weight

85 differently than proteins; for example, the MG conjugate to a 1 kDa PEG chain with a
86 molecular weight of 1.55 kDa behaved in solution like a 4.3 kDa protein. Because the
87 hydrodynamic size of fluorogens was not taken into account previously, here sizes are
88 expressed in terms of apparent protein molecular weights. Specifically, a series of
89 unbranched MG-PEGs with apparent protein molecular weights ranging from 4.3 to 71.1
90 kDa were examined for activity-evoked FAP responses at *Drosophila* muscle 6/7 NMJ
91 type Ib boutons. As demonstrated with other membrane impermeant fluorogens such as
92 MG-BTau, FAP responses reflect the opening of fusion pores and the retention of
93 fluorescent MG-Dilp2-FAP complexes that do not exit through fusion pores (Bulgari *et*
94 *al.*, 2019).

95 Responses to 1 minute of 70 Hz stimulation led to robust labeling with the 4.3
96 kDa fluorogen, but were attenuated with larger fluorogens (Fig. 1A-D). For the three
97 smaller fluorogens (4.3, 12.5 And 32.4 kDa), the incremental changes could reflect the
98 slower diffusion of larger fluorogens and the effect of approaching the size cutoff of the
99 fusion pore, which is well suited for release of *Drosophila* neuropeptides. However, the
100 two largest fluorogens (53.2 and 71.1 kDa), with incrementally modest increases in
101 hydrodynamic size (because radius is proportional to the cube root of protein molecular
102 weight), barely produced any signals (Fig. 1C,D), thereby indicating poor permeation
103 through synaptic DCV fusion pores that open in response to $Ca^{2+}$ elevation induced by
104 activity. With spontaneous fusion pore openings (Bulgari *et al.*, 2019), the same
105 properties are evident: in contrast with the 4.3 and 32.4 kDa fluorogens, time-
106 dependent labeling was not seen with incubation of the NMJ with the 53.2 kDa
107 fluorogen in the absence of $Ca^{2+}$ for 8 minutes (Fig. 1E,F,G). Thus, synaptic fusion pore

108 permeability is sufficient for the release of *Drosophila* neuropeptides, but excludes DCV
109 cargos that exceed the fusion pore cutoff, which falls between 32.4 and 53.2 kDa.
110
111 *Frequency of DCV emptying events*
112 Given the above synaptic DCV fusion pore permeability, we explored whether
113 NMJ DCVs ever empty to efficiently release large cargos, a process often referred to as
114 full fusion (FF). For this purpose, 1 μM MG-BTau was used to detect spontaneous
115 events that occur in the absence of extracellular $Ca^{2+}$ (Bulgari *et al.*, 2019), thus
116 enabling imaging of individual release sites without interference from surrounding
117 events that are stimulated by activity. Single labeling events via kiss and run fusion
118 pores (Fig. 2A, K&R) were readily detected by their sustained labeling and occurred
119 with variable kinetics (Fig. 2B, top and middle); overall, they grew over 23.7 $\pm$ 2.7
120 seconds (n = 37) and could persist for the duration of imaging (up to 4 minutes).
121 However, on rare occasions labeling via the opening of a fusion pore was followed
122 within seconds by the rapid loss of fluorescence (Fig. 2A, FF). Again, time courses were
123 variable (Fig. 2C); the lifetime of these events was 17.25 $\pm$ 3.81 seconds with a rise time
124 to peak fluorescence of 5.62 $\pm$ 0.53 seconds (n=8). Based on the imaging field of view
125 and the depth of field, such events could not be attributed to undocking and transport of
126 DCVs. Rather, following MG fluorogen influx through the fusion pore and binding to the
127 FAP, MG-FAP complexes that normally are retained (i.e., cannot exit through fusion
128 pores) must have been released by fusion pore dilation that resulted in DCV emptying.
129 Interestingly, such full fusions could occur with a DCV that had already had a kiss and
130 run event (Fig. 2C, bottom). Overall, DCV full fusions only occurred in 3.6% of

131 exocytotic events at the synapse in these experiments (Fig. 3A, Con; filled bar shows
132 kiss and run, open bar shows full fusion; frequencies expressed per bouton).
133
134 *cAMP evokes opening of dilating fusion pores*
135 Because it seems unlikely that such rare full fusions wholly account for release of
136 large DCV cargo proteins, we considered that signaling might trigger synaptic DCV full
137 fusions. A candidate for such a trigger is cAMP, which evokes $Ca^{2+}$ independent release
138 from DCVs at the *Drosophila* NMJ (Shakiryanova *et al.*, 2011; Bulgari *et al.*, 2018).
139 Therefore, we tested whether cAMP in the absence of extracellular $Ca^{2+}$ affects the
140 frequency of kiss and run and/or full fusions.
141 Four independent experimental approaches showed that cAMP selectively
142 evokes presynaptic DCV full fusions. First, the membrane permeant cAMP analog 8-
143 parachlorophenyl-thio-cAMP (CPT, 1 mM) increased the frequency of full fusions
144 without affecting kiss and run events (Fig. 3A). Second, bath application of 100 μM
145 octopamine, an insect neuromodulator that acts via cAMP to promote the growth of
146 NMJ arbors (Koon *et al.*, 2011), also increased the frequency of DCV emptying with no
147 effect on the kiss and run event frequency (Fig. 3A, Oct). Third, bath application of 100
148 μM forskolin (FSK), an adenylate cyclase activator, increased the full fusion frequency
149 without altering kiss and run fusions frequency (Fig. 3B) or the rise times of responses
150 (25.5 $\pm$ 3 s (n = 23) for kiss and run; 6.0 $\pm$ 1.0 (n = 11) for full fusions). Thus, frequency
151 of one subtype of release is affected without changing kinetics of individual events.
152 Finally, following motor neuron specific expression of the photoactivatable adenylate
153 cyclase PACα (Schröder-Lang et al, 2007), blue light activation of the adenylate cyclase

154 increased the frequency of DCV full fusions, again with no change in kiss and run
155 frequency (Fig. 3C). Together, these results reveal that cAMP evokes release from
156 presynaptic DCVs by selectively increasing the frequency of full fusions without
157 affecting ongoing kiss and run exocytosis.
158
159 *Anchored PKA-R2 is required for cAMP-evoked full fusions*
160 The effects of cAMP are mediated by two ubiquitously expressed intracellular
161 cAMP effectors, protein kinase A (PKA) and the exchange protein directly activated by
162 cAMP (Epac) (de Rooij, 1998). To test for a role of Epac, we began with bath application
163 of the Epac activator 8-(4-methoxyphenylthio)-2′-O-methyl-cAMP (Me, 200 μM).
164 However, no changes in the frequencies of emptying or kiss and run events were
165 produced (Fig. 4A,D). Furthermore, pretreatment of boutons with Epac inhibitor ESI-09
166 (10 μM) did not disrupt the forskolin-evoked increase in full fusion frequency (Fig. 4B) or
167 alter kiss and run events (Fig. 4E). Finally, in Epac null animals (Shakiryanova *et al.*,
168 2011), which have a P element insertion near the C-terminal cyclic nucleotide-binding
169 domain, the selective effect of forskolin on emptying persisted (Fig. 4C,F). Interestingly,
170 the latter two approaches to reducing epac function tended to increase basal emptying
171 frequency without eliminating the forskolin effect. This suggests that epac may constrain
172 fusion pore dilation in the synaptic terminal independently of cAMP. But more important
173 here, Epac is not required for cAMP-induced DCV full fusions.
174 In contrast, presynaptic PKA containing the type 2 regulatory subunit (PKA-R2) is
175 required for cAMP-evoked DCV full fusions. First, the PKA catalytic subunit inhibitor H89
176 (20 μM) blocks the forskolin-induced full fusions (Fig. 5A, open bars) without altering kiss

177 and run events (Fig. 5A, filled bars). Second, presynaptic expression of a PKA-R1
178 dominant negative subunit failed to affect the cAMP effect (Fig. 5B), consistent with the
179 involvement of PKA-R2. Third, knockdown of PKA-R2 inhibited the cAMP effect. For
180 these experiments, initial attempts to express Dilp2-FAP and a PKA-R2 RNAi with the
181 motor neuron driver OK6-GAL4 did not produce viable progeny. Therefore, PKA-R2
182 RNAi was expressed only in type Ib boutons with the Dip-β-GAL4 driver (Wang *et al*,
183 2022). Strikingly, the forskolin effect on emptying frequency was eliminated, while kiss
184 and run events were unchanged (Fig. 5C,D). We also tested the role of PKA-R2 in type
185 Is boutons using the ShakB-GAL4 driver. Forskolin produced the same phenomenon of
186 increased emptying frequency in type Is boutons as found in Ib boutons (Fig. 5E) and
187 this effect was also inhibited by PKA-R2 RNAi knockdown, again without affecting kiss
188 and run events (Fig. 5F). Finally, we focused on the association of PKA-R2 with AKAPs
189 (A-kinase anchoring proteins). Acute treatment of NMJs with 20 μM St-Ht31, a stearated
190 membrane permeant inhibitor of the interaction of PKA-R2 with AKAPs (Vijayaraghavan
191 *et al.*, 1997), abolished the facilitating effect of FSK on DCV full fusions with no effect on
192 kiss and run frequency (Fig. 5G). This short-term experiment further implicates PKA-R2
193 without confounding developmental effects. However, this result cannot localize the
194 interaction of PKA-R2 and AKAP interaction to the presynaptic neuron (as opposed to
195 the postsynaptic muscle). Therefore, RNAi knockdown of *Drosophila* Rugose (also called
196 Akap550), a neuronal PKA-R2 anchor (Han *et al.*, 1997), was induced in motor neurons.
197 This genetic presynaptic perturbation inhibited the effect of cAMP on DCV full fusions,
198 again without affecting kiss and run exocytosis frequency (Fig. 5H). Taken together,
199 these experimental results demonstrate that cAMP activation of anchored PKA-R2

200 triggers $Ca^{2+}$-independent full fusion of presynaptic DCVs.

201

202 *Complexin participates in cAMP-evoked release from synaptic DCVs*

203 The above results pose the question of how rugose-anchored PKA activity
204 induces $Ca^{2+}$-independent synaptic DCV full fusions. Recent findings directed our
205 attention to complexin (Cpx), which is often referred to as fusion clamp because it
206 reduces spontaneous SSV fusion. First, spontaneous release from DCVs and SSVs are
207 similar at the NMJ: both persist in the presence of tetanus toxin and share SNARE
208 dependence (Bulgari *et al.*, 2019). Furthermore, *Drosophila* complexin is
209 phosphorylated by PKA at S126 to upregulate (or unclamp) spontaneous SSV release
210 events (Cho *et al.*, 2015). Therefore, the increase in spontaneous DCV release events
211 with cAMP could be accounted for by complexin phosphorylation. Second, *in vitro*
212 reconstitution experiments devoid of much of the cellular exocytosis machinery suggest
213 the potential for facilitation of fusion pore dilation by complexin (Pierson and Shin,
214 2021). Together, these observations support the hypothesis that complexin S126 is
215 required for $Ca^{2+}$-independent PKA-induced spontaneous DCV full fusions.

216 Therefore, we examined the effect of replacing native complexin with the
217 unphosphorylatable S126A mutant ($Cpx^{S126A}$) by rescuing a Cpx null mutant with
218 neuronal expression of $Cpx^{S126A}$ (i.e., as in Cho *et al.*, 2015). First, to test whether the
219 mutant rescue was effective for DCVs, a GFP-tagged neuropeptide (ANF-GFP) (Rao *et*
220 *al.*, 2001) that reports native DCV-mediated release (e.g., Husain and Ewer, 2004) was
221 expressed while replacing Cpx with $Cpx^{S126A}$ and release was measured as the loss of
222 ANF-GFP fluorescence. In the presence of extracellular $Ca^{2+}$, activity-evoked DCV-

223 mediated release in $Cpx^{S126A}$ animals was intact: the ~20% release (Fig. 6A), followed
224 by some recovery due to activity-dependent capture, matches prior control responses
225 with GFP imaging (Shakiryanova *et al.*, 2005, 2006; Wong *et al.*, 2015; Cavolo *et al.*,
226 2016). Thus, the $Cpx^{S126A}$ complexin mutant supports $Ca^{2+}$ dependent synaptic DCV
227 exocytosis.

228 Then cAMP-evoked release was measured in the absence of extracellular $Ca^{2+}$.
229 Figure 6B shows that the ANF-GFP release response to forskolin is abolished in
230 $Cpx^{S126A}$ animals: with the mutant the minor change in fluorescence that occurred with
231 forskolin matched the photobleaching control. Finally, FAP imaging was used to
232 measure the impact of $Cpx^{S126A}$ on DCV full fusions (Fig. 6C). As expected from all
233 previous experiments, no change occurred in kiss and run frequency. Furthermore, in
234 accordance with ANF-GFP experiments, cAMP stimulation of DCV full fusions was
235 abolished (i.e., the open bars in Fig. 5C were not significantly different, ns). Therefore,
236 reminiscent of SSVs, complexin's PKA phosphorylation site is needed for the cAMP-
237 induced increase in frequency of spontaneous DCV-mediated release. However,
238 complexin S126 has the added impact for DCVs of supporting cAMP-evoked opening of
239 dilating fusion pores to enable release of proteins that are too large to permeate through
240 the fusion pores that normally dominate release.

241

242 **DISCUSSION**

243 Neuronal DCVs are distinguished by their small size relative to the best studied
244 endocrine DCVs, widely varying contents within a single cell and, at a native intact
245 synapse, the nearly exclusive use of fusion pores formed by dynamin dependent kiss

246 and run exocytosis for spontaneous and activity-evoked release (Wong *et al.*, 2015;
247 Bulgari *et al.*, 2019, Fig. 3A). The resultant partial release from DCVs fits with the need
248 to preserve presynaptic DCVs, which can only be replaced very slowly by axonal
249 transport, but posed the question of whether large DCV cargos can permeate through
250 fusion pores. FAP imaging with a series of PEGylated fluorogens provided a means to
251 determine the conduction properties of synaptic DCV fusion pores without cargo specific
252 confounds that affect release (e.g., binding to luminal DCV constituents). The
253 experimental data presented here establish that presynaptic DCV fusion pores are large
254 enough to release all *Drosophila* neuropeptides, but insufficient for large proteases that
255 undergo activity-dependent synaptic release (e.g., TPA and neurotrypsin). However,
256 this limit is bypassed by cAMP-induced $Ca^{2+}$-independent full fusions. The resultant
257 efficient release of large cargos may contribute to developmental growth and refinement
258 of NMJ terminals, which depend on cAMP (Zhong *et al.*, 1992; Koon *et al.*, 2011;
259 Vonhoff and Keshishian, 2017).

260 cAMP-evoked DCV emptying (Fig. 3) requires PKA-R2 and its anchor Rugose
261 (Fig. 5). cAMP also stimulates spontaneous release from SSVs at the *Drosophila* NMJ
262 (Yoshihara *et al.*, 1999; Zhang *et al.*, 1999; Cho *et al.*, 2015), but the role of Rugose has
263 not been examined for SSVs. However, Rugose affects larval NMJ morphology and a
264 variety of adult behaviors including associative learning (Volders *et al.*, 2012; Wise *et*
265 *al.*, 2015). Because Rugose and its mammalian ortholog Neurobeachin, a candidate
266 autism gene (Castermans *et al.*, 2003), are localized near the trans Golgi network
267 (Wang *et al.*, 2000; Volders *et al.*, 2012), effects on synapses and behavior have been
268 proposed to originate from perturbing the somatodendritic compartment (e.g., by

269 affecting Golgi function, postsynaptic receptors and dendritic spines) (Niesmann *et al.*,
270 2011; Volders *et al.*, 2012; Gromova *et al.*, 2018; Repetto *et al.*, 2018). However, the
271 effect of acute disruption of the PKA-R2 anchoring on cAMP-induced full fusions at
272 boutons (Fig. 5G) establishes that Rugose is present and functions in presynaptic
273 boutons. Thus, cAMP-induced spontaneous synaptic release by DCVs and possibly
274 SSVs involving Rugose/Neurobeachin-anchored PKA-R2 may locally control synaptic
275 release to influence behavior.

276 One way the regulation of fusion could be represented is with a channel gating
277 model in which the fusion pore moves between closed (C), open (O) and dilated (D)
278 states ($C \rightleftharpoons O \rightarrow D$). In this scheme, reaching only the O state results in kiss and run
279 release, while reaching the D state produces full fusion (i.e., DCV emptying). If the
280 cAMP/PKA/complexin pathway selectively increased the number of fusions by
281 promoting the $C \rightarrow O$ step, the frequency of kiss and run events, as well as subsequent
282 emptying events, would have increased. Yet kiss and run frequency did not increase in
283 response to cAMP, thus excluding this possibility. An alternative hypothesis is that
284 cAMP/PKA/complexin pathway increases the incidence of dilation, which initiates full
285 fusion (the $O \rightarrow D$ step). With this mechanism, would-be kiss and run release events
286 are converted to full fusions. Therefore, the greater frequency of full fusions would be
287 accompanied with a reduced frequency of kiss and run events. But this was not found,
288 thereby showing cAMP-induced full fusions are not produced at the expense of kiss and
289 run events. Instead, rugose-anchored PKA increases total fusion pore openings with the
290 “extra” events being committed to fusion pore dilation. With simple gating models
291 eliminated, the selective increase in spontaneous full fusions reported here is consistent

292 with complexin phosphorylation both unclamping DCVs normally held in reserve (thus
293 recruiting “extra” DCVs to undergo $Ca^{2+}$-independent exocytosis) and dilating resultant
294 fusion pores. With pore dilation, large cargos that do not readily pass through activity-
295 evoked fusion pores are released. Thus, diverse triggers ($Ca^{2+}$ elevation induced by
296 activity and complexin phosphorylation induced by rugose-anchored PKA) evoke
297 release of distinct DCV cargos by opening differentially dilated fusion pores.
298

299 **MATERIALS AND METHODS**

300 **Imaging.** *Drosophila melanogaster* third instar larvae were filleted and imaged in $Ca^{2+}$-
301 free HL3 in which 1.5 mM $Ca^{2+}$ was substituted with 0.5 mM EGTA, a $Ca^{2+}$ chelator (70
302 mM NaCl, 5 mM KCl, 0.5 mM $Na_3EGTA$, 20 mM $MgCl_2$, 10 mM $NaHCO_3$, 5 mM
303 trehalose, 115 mM sucrose, 5 mM hemi-sodium HEPES, pH 7.25). For electrical
304 stimulation experiments they were transferred to HL3 saline that contained (in mM) 70
305 mM NaCl, 5 KCl, 1.5 $CaCl_2$, 20 $MgCl_2$, 10 $NaHCO_3$, 5 trehalose, 115 sucrose, and 5
306 hemi-sodium HEPES, pH 7.25 supplemented with 10 mM L-glutamate to prevent
307 muscle contractions. Nerve terminals were stimulated at 70 Hz for 1 minute via
308 segmental nerves with a suction electrode (Shakiryanova et al, 2005). Dilp2-FAP data
309 were acquired in muscle 6/7 type I boutons of with an upright Olympus microscope
310 equipped with a 60×1.1 NA water immersion objective, a Yokogawa CSU-X1 spinning
311 disk confocal head, a Coherent Obis 640 nm laser for fluorogen illumination, a Ludl filter
312 wheel with an ET 700/75 emission filter and a Teledyne Photometrics Prime 95B
313 sCMOS camera. ANF-GFP type Ib bouton data were acquired as described previously
314 (Levitan et al, 2007; Wong *et al.*, 2015). PACα photoactivation in synaptic boutons was

315 achieved by illuminating synaptic boutons with 488 nm light for 300 ms at 0.33 Hz for
316 the whole duration of FAP imaging (4 minutes). Quantification of fluorescence intensity
317 was performed with ImageJ software (https://imagej.nih.gov/ij/) as previously described
318 (Levitan et al, 2007). Spontaneous fusion events were counted manually from time-
319 lapse images taken for 4 min at 0.33 or 0.5 Hz. Statistical analysis and graphing were
320 performed with GraphPad Prism software. Error bars represent SEM. Statistical
321 significance was determined with Student's t-test for two experimental groups and
322 ANOVA with Dunnett's or Tukey's post-test for more experimental groups.
323 **Reagents.** For synthesis of MG-PEGs, commercially available mPEG-azides of sizes
324 1K, 2K, 5K, 10K and 20 K (Biochempeg Scientific Inc.) were coupled to MG-EDA-alkyne
325 via click reaction (Szent-Gyorgyi *et al.*, 2023). Hydrodynamic sizes in terms of apparent
326 protein molecular weights were determined by FPLC with a HiPrep 26/60 Sephacryl S-
327 200 high-resolution column with protein standards ranging from 6.5 to 66.5 kDa
328 (aprotinin, cytochrome C, carbonic anhydrase, albumin). Resultant apparent protein
329 molecular weights were: 4.3 kDa for MG-PEG1K, 12.5 kDa for MG-PEG2K, 32.4 kDa
330 for MG-PEG5K, 53.2 kDa for MG-PEG10K and 71.1 kDa for MG-PEG20K. MG-PEG
331 conjugates and MG-BTau were used at 1 μM final concentration in imaging
332 experiments. Octopamine and MG-BTau were bath applied immediately before imaging.
333 Time-lapse images were taken for 4 minutes at 0.3 or 0.5 Hz. Boutons were treated with
334 8-parachlorophenyl-thio-cAMP and 8-(4-methoxyphenylthio)-2′-O-methyl-cAMP for 15
335 minutes before application of 1 μM MG-BTau followed by image sequence acquisition.
336 stHT-31, ESI-09 and H-89 were applied for 15 to 20 min before application of forskolin,
337 then imaged 3 minutes after forskolin exposure in the presence of MG-BTau. Forskolin

338 was dissolved in DMSO as stock and subsequently diluted to yield a final concentration
339 of DMSO of 0.1%. An equivalent amount of the vehicle was used as the matched
340 control. Forskolin, 8-parachlorophenyl-thio-cAMP and ESI-09 were from Sigma, 8-(4-
341 methoxyphenylthio) -2′-O-methyl-cAMP from Biolog Life Sciences, H-89 from Cayman
342 Chemicals and St-Ht31 from Fisher Scientific.
343 **Flies.** UAS-Dilp2-FAP and UAS-ANF-GFP flies were described previously (Rao *et al.*,
344 2001; Bulgari *et al.*, 2019). Epac function was disrupted based a P-element insertion in
345 the gene (Epac KG00434; Bloomington stock #13663). Other Bloomington stocks used
346 were: OK6-GAL4 (#64199), DIPβ-GAL4 (#90316), UAS-PACα (#78790), the dominant
347 negative PKA-R1 UAS-PKA.R1BDK (#35550), UAS-PKA-R2 RNAi (#53930), Valium20
348 RNAi control (#35783), UAS-rugose RNAi (#57703) and the complexin null $Cpx^{Delta2}$
349 (#64252). The ShakB-GAL4 line was from Tanja Godenschwege (Florida Atlantic
350 University). J. Troy Littleton (MIT) provided elav-GAL4;;UAS-$Cpx^{S126A}$, $Cpx^{SH1}$/TM6B,Tb
351 flies, with $Cpx^{SH1}$ being a complexin null mutant.
352
353 **Acknowledgements:** We thank Drs. Tanja Godenschwege (Florida Atlantic
354 University), Robert A. Carrillo (University of Chicago) and J. Troy Littleton
355 (Massachusetts Institute of Technology) for flies, and Drs. Manfred Lindau (University of
356 Miami), Ronald Holz (University of Michigan) and Christopher Szent-Gyorgyi (Carnegie
357 Mellon University) for helpful discussions.
358
359 This research was supported by the National Institutes of Health grant R01 NS032385
360 to ESL.

361 **REFERENCES**

362

363 Anantharam A, Bittner MA, Aikman RL, Stuenkel EL, Schmid SL, Axelrod D, Holz RW.
364 A new role for the dynamin GTPase in the regulation of fusion pore expansion. *Mol Biol*
365 *Cell.* **22**, 1907-18 (2011).

366

367 Baranes D, *et al.* Tissue plasminogen activator contributes to the late phase of LTP and
368 to synaptic growth in the hippocampal mossy fiber pathway. *Neuron* **21**, 813-25 (1998).

369

370 Bulgari D, *et al.*, Activity-evoked and spontaneous opening of synaptic fusion pores.
371 *Proc. Natl. Acad. Sci. U.S.A.* **116**, 17039–17044 (2019).

372

373 Bulgari D., Jha A., Deitcher D. L., Levitan E.S. Myopic (HD-PTP, PTPN23) selectively
374 regulates synaptic neuropeptide release. *Proc Natl Acad Sci U S A.* **115**, 1617-1622
375 (2018).

376

377 Castermans D, *et al.* The neurobeachin gene is disrupted by a translocation in a patient
378 with idiopathic autism. *J Med Genet.* **40**, 352-6 (2003).

379

380 Cavolo SL, Bulgari D, Deitcher DL, Levitan ES. Activity Induces Fmr1-Sensitive
381 Synaptic Capture of Anterograde Circulating Neuropeptide Vesicles. *J Neurosci.* **36**,
382 11781-11787 (2016).

383

384 Cho RW, *et al.* Phosphorylation of Complexin by PKA Regulates Activity-Dependent
385 Spontaneous Neurotransmitter Release and Structural Synaptic Plasticity. *Neuron* **88**,
386 749-61 (2015).
387
388 J de Rooij, *et al.* Epac is a Rap1 guanine-nucleotide-exchange factor directly activated
389 by cyclic AMP. *Nature* **396**,474-7 (1998).
390
391 Gromova KV, *et al.* Neurobeachin and the kinesin KIF21B are critical of endocytic
392 recycling of NMDA receptor and regulate social behavior. *Cell Rep.* **23**, 2705-2717
393 (2018).
394
395 Han JD, Baker NE, Rubin CS. Molecular characterization of a novel A kinase anchor
396 protein from Drosophila melanogaster. *J Biol. Chem.* **272,** 26611-9 (1997).
397
398 Huang YY *et al.* Mice lacking the gene encoding tissue-type plasminogen activator
399 show a selective interference with late-phase long-term potentiation in both Schaffer
400 collateral and mossy fiber pathways. *Proc Natl Acad Sci U S A.* **93**, 8699-704. (1996).
401
402 Husain QM, Ewer J. Use of targetable gfp-tagged neuropeptide for visualizing
403 neuropeptide release following execution of a behavior. *J. Neurobiol.* **59**, 181-91 (2004).
404
405 Koon AC, *et al.* Autoregulatory and paracrine control of synaptic and behavioral
406 plasticity by octopaminergic signaling. *Nat Neurosci.* **14**,190-9 (2011).

407

408 Levitan ES, Lanni F, Shakiryanova D. *In vivo* imaging of vesicle motion and release at
409 the Drosophila neuromuscular junction. *Nat Protoc.* **2**, 1117-25 (2007).
410

411 Niemann K, *et al.* Dendritic spine formation and synaptic function require Neurobeachin.
412 *Nat Comm.* **2**, 557 (2011).
413

414 Pierson J, Shin YK. Stabilization of the SNARE core by Complexin-1 facilitates fusion
415 pore expansion. *Front. Mol. Biosci.* **8**, 805000 (2021).
416

417 Rao S, Lang C, Levitan ES, Deitcher DL. Visualization of neuropeptide expression,
418 transport, and exocytosis in Drosophila melanogaster. *J. Neurobiol.* **49**, 159-172 (2001).
419

420 Repetto D, *et al.* Molecular dissection of Neurobeachin function at excitatory synapses.
421 *Front. Synaptic Neurosci.* **10**, 28 (2018).
422

423 Schröder-Lang S, *et al.* Fast manipulation of cellular cAMP level by light in vivo
424 *Nat Methods* **4**, 39-42 (2007).
425

426 Shakiryanova D, Tully A, Hewes RS, Deitcher DL, Levitan ES. Activity-dependent
427 liberation of synaptic neuropeptide vesicles. *Nat Neurosci.* **8**, 173-8 (2005).
428

429 Shakiryanova D, Tully A, Levitan ES. Activity-dependent synaptic capture of transiting

430 peptidergic vesicles. *Nat. Neurosci.* **9**, 896-9000 (2006).

431

432 Shakiryanova D., Zettel G. M., Gu T., Hewes R. S., Levitan E. S. Synaptic neuropeptide
433 release induced by octopamine without $Ca^{2+}$ entry into the nerve terminal. *Proc Natl*
434 *Acad Sci U S A.* **108**, 4477-4481 (2011).

435

436 Sharma S, Lindau M. The fusion pore, 60 years after the first cartoon. *FEBS Lett.* **592**,
437 3542-3562 (2018).

438

439 Szent-Gyorgyi C., et al. Bottom-Up design: a modular golden gate assembly platform of
440 yeast plasmids for simultaneous secretion and surface display of distinct FAP fusion
441 proteins. *ACS Synth Biol.* **11**, 3681-3698 (2022).

442

443 Takahashi N., Kishimoto T., Nemoto T., Kadowaki T., Kasai H. Fusion pore dynamics
444 and insulin granule exocytosis in the pancreatic islet. *Science* **297**, 1349-52 (2002).

445

446 Vijayaraghavan S, Goueli SA, Davey MP, Carr DW. Protein kinase A-anchoring inhibitor
447 peptides arrest mammalian sperm motility. *J Biol Chem.* **272**, 4747-52 (1997).

448

449 Volders K, *et al.* Drosophila rugose is a functional homolog of mammalian
450 Neurobeachin and affects synaptic architecture, brain morphology, and associative
451 learning. *J Neurosci.* **32**, 15193-204 (2012).

452

453 Vonhoff F, Keshishian H. Cyclic nucleotide signaling is required during synaptic
454 refinement at the Drosophila neuromuscular junction. *Dev. Neurobiol.* **77**, 39-60 (2017).
455
456 Wang X, *et al.* Neurobeachin: A protein kinase A-anchoring, beige/Chediak-higashi
457 protein homolog implicated in neuronal membrane traffic. *J Neurosci.* **20**, 8551-65
458 (2000).
459
460 Wang Y, *et al*. Systematic expression profiling of Dpr and DIP genes reveals cell
461 surface codes in Drosophila larval motor and sensory neurons. *Development* **49**,
462 dev200355 (2022).
463
464 Wise A, *et al.* Drosophila mutants of the autism candidate gene neurobeachin (rugose)
465 exhibit neuro-developmental disorders, aberrant synaptic properties, altered locomotion,
466 and impaired adult social behavior and activity patterns. *J Neurogenet.* **29**, 135-43
467 (2015).
468
469 Wong M. Y., Cavolo S. L., Levitan E. S., Synaptic neuropeptide release by dynamin-
470 dependent partial release from circulating vesicles. *Mol. Biol. Cell* **26**, 2466–2474
471 (2015).
472
473 Yoshihara M, *et al.* Selective effects of neuronal-synaptobrevin mutations on transmitter
474 release evoked by sustained versus transient $Ca^{2+}$ increases and by cAMP. *J Neurosci.*
475 **19**, 2432-41 (1999).

476

477 Zhang D, Kuromi H, Kidokoro Y. Activation of metabotropic glutamate receptors

478 enhances synaptic transmission at the Drosophila neuromuscular junction.

479 *Neuropharmacology* **38**, 645-57 (1999).

480 Zhong Y, Budnik V, Wu CF. Synaptic plasticity in Drosophila memory and

481 hyperexcitable mutants: role of cAMP cascade. *J Neurosci.***12**, 644-51 (1992).

482

483 **LEGENDS**

484

485 **Fig. 1. Permeability of PEG derivatives through DCV fusion pores.**

486 Contrast-enhanced fluorescent images of type Ib boutons from Ok6-GAL4 UAS-Dilp2FAP

487 larvae before and after 70 Hz stimulation for 60 s in the presence of 4.3 kDa (**A**), 32.4 kDa

488 (**B**) and 53.2 kDa (**C**) MG-PEG dyes, each at 1 μM. Anti-horseradish peroxidase

489 immunofluorescence (HRP) is shown to indicate location of boutons. (**D**) Time-course of

490 activity-evoked FAP responses in the presence of MG-PEG dyes normalized to initial

491 labeling. Apparent protein sizes shown in symbol labels. Black bar, 70 Hz stimulation. 4.3

492 kDa (n=8), 12.5 kDa (n=7), 32.4 kDa (n=5), 53.2 kDa (n=6), 71.1 kDa (n=6). Contrast-

493 enhanced fluorescent images of Dilp2-FAP expressing boutons in the absence of $Ca^{2+}$ after

494 application of 4.3 kDa (**E**), 32.4 (**F**) and 53.2 kDa (**G**) MG-PEGs. Numbers on the images

495 indicate time in minutes. White scale bars, 2 μm.

496

497 **Fig. 2. Individual spontaneous kiss and run and full fusion events.**

498 (**A**) Contrast-enhanced fluorescent images of single labeled Dilp2-FAP presynaptic sites in

499 the absence of $Ca^{2+}$ after application of MG-BTau fluorogen in OK6>Dilp2-FAP type Ib
500 boutons. Upper panels labeled K&R show consecutive images of kiss and run pore
501 opening, while the lower panels labeled FF show consecutive images of full fusion pore
502 dynamics. Numbers on images indicate times in seconds. Scale bar, 1 μm. Normalized
503 time courses of representative individual (**B**) kiss and run and (**C**) full fusion sites.
504
505 **Fig. 3. cAMP increases the frequency of spontaneous full fusions.**
506 (**A**) Frequency of kiss and run (filled bars) and full fusions (open bars) in control boutons
507 (Con, n=8), boutons treated with the cAMP agonist 8-parachlorophenyl-thio-cAMP (Cpt,
508 n=7) or boutons treated with octopamine (Oct, n=11) in the presence of MG-BTau.
509 Statistical comparisons are always between like colored bars; **$p < 0.01$, ***$p < 0.001$,
510 Dunnett's posttest following one-way ANOVA. (**B**) Frequency of kiss and run (filled bars)
511 and full fusions (open bars) per bouton in DMSO control (Con, n=12) and FSK treated
512 neurons (FSK, n=17) in the presence of MG-BTau, **$p < 0.01$, unpaired t-test. (**C**)
513 Frequency of kiss and run (filled bars) and full fusions (open bars) in PACα expressing
514 boutons without illumination (-Light, n=11) and light-activated PACα (+Light, n=16) in the
515 presence of MG-BTau, Statistical comparisons are always between like colored bars; *$p <$
516 $0.05$, unpaired t-test. There were no significant differences between kiss and run fusions
517 frequency (filled bars) in presented experiments, unpaired t-test. All data derived from Ib
518 boutons of OK6>Dilp2-FAP animals.
519
520 **Fig. 4. Epac is not involved in cAMP-induced full fusions.**
521 (**A**) Frequency of full fusions in presence of MG-BTau in control OK6>Dilp2-FAP boutons

522 (Con, n=12) and pretreated with Epac activator 8-(4-methoxyphenylthio)-2′-O-methyl-cAMP
523 (Me, n=7). No significant difference was detected with unpaired t-test. (**B**) Epac inhibitor
524 ESI-09 without FSK (-FSK, n=10,) and with FSK (+FSK, n=7), ***p < 0.001. (**C**) in flies
525 expressing Epac null without FSK (-FSK, n=11) and with FSK (+FSK, n=17), ***p < 0.001.
526 (**D-F**) Frequency of kiss and run fusions with conditions corresponding to **A-C.** Note that
527 there were no significant differences in kiss and run fusions for the experimental conditions
528 presented here.
529
530 **Fig. 5. cAMP-induced full fusions require anchored PKA-R2.**
531 (**A**) Frequency of kiss and run (filled columns) and full fusions (open columns) in
532 OK6>Dilp2-FAP boutons treated with H89 without (-FSK, n=14) and with FSK application
533 (+FSK, n=9). (**B**) Frequency of fusions in OK6>Dilp2-FAP boutons coexpressing dominant-
534 negative PKA-R1 (-FSK, n=8; +FSK, n=14) **p < 0.01. Frequency of fusions in (**C**) DIPβ-
535 GAL4>Dilp2-FAP boutons (n=8; +FSK, n=9, **p < 0.01) and (**D**) DIPβ-GAL4>Dilp2-FAP
536 boutons also expressing PKA-R2 RNAi (-FSK, n=7; +FSK, n=7). (**E**) ShakB-GAL4>Dilp2-
537 FAP coexpressing the UAS-Valium20 RNAi control with and without FSK treatment (-FSK,
538 n=8; +FSK, n=10) and (**F**) ShakB-GAL4>Dilp2-FAP boutons coexpressing UAS-PKA-R2
539 RNAi with and without FSK treatment (-FSK, n=8; +FSK, n=19). (**G**) Frequency of fusions in
540 St-Ht31 pretreated OK6>Dilp2-FAP boutons with and without FSK treatment (-FSK, n=12),
541 (+FSK, n=20). (**H**) Frequency of fusions in OK6>Dilp2-FAP boutons coexpressing UAS-
542 rugose with and without FSK (-FSK, n=13; +FSK, n=11). No significant difference was
543 found between kiss and run fusions frequency in FSK-treated and non-treated boutons,
544 unpaired t-test.

545 **Fig. 6. The complexin S126 PKA phosphorylation site is required for cAMP-evoked**
546 **full fusions and neuropeptide release.**
547 (**A**) Release indicated by loss of ANF-GFP fluorescence is induced by a 1 minute 70 Hz
548 stimulation (indicated by the horizontal bar) in elav-GAL4 UAS-ANF-GFP;;UAS-$Cpx^{S126A}$,
549 $Cpx^{SH1}$ animals (n=4). (**B**) Forskolin evoked ANF-GFP release in 7 minutes is abolished in
550 elav-GAL4 UAS-ANF-GFP;;UAS-$Cpx^{S126A}$, $Cpx^{SH1}$ animals. WT, wild type Cpx; PB Con,
551 photobleaching control. n=4-6, ****$p < 0.0001$, Tukey's test following ANOVA. (**C**)
552 Frequency of kiss and run (filled columns) and full fusions (open columns) in boutons from
553 elav-GAL4;UAS-Dilp2-FAP;UAS-$Cpx^{S126A}$, $Cpx^{SH1}$/$Cpx^{Delta2}$ flies in the absence and
554 presence of forskolin (-FSK (n=7) and +FSK (n=14), respectively). $Cpx^{SH1}$ and $Cpx^{Delta2}$ are
555 null mutants. Note that forskolin does not have a statistically significant effect (ns, not
556 significant by t-test) on full fusion frequency (open bars). Likewise, no effect was produced
557 on kiss and run frequency.

**Figure 1.** Permeability of PEG derivatives through fusion pores.

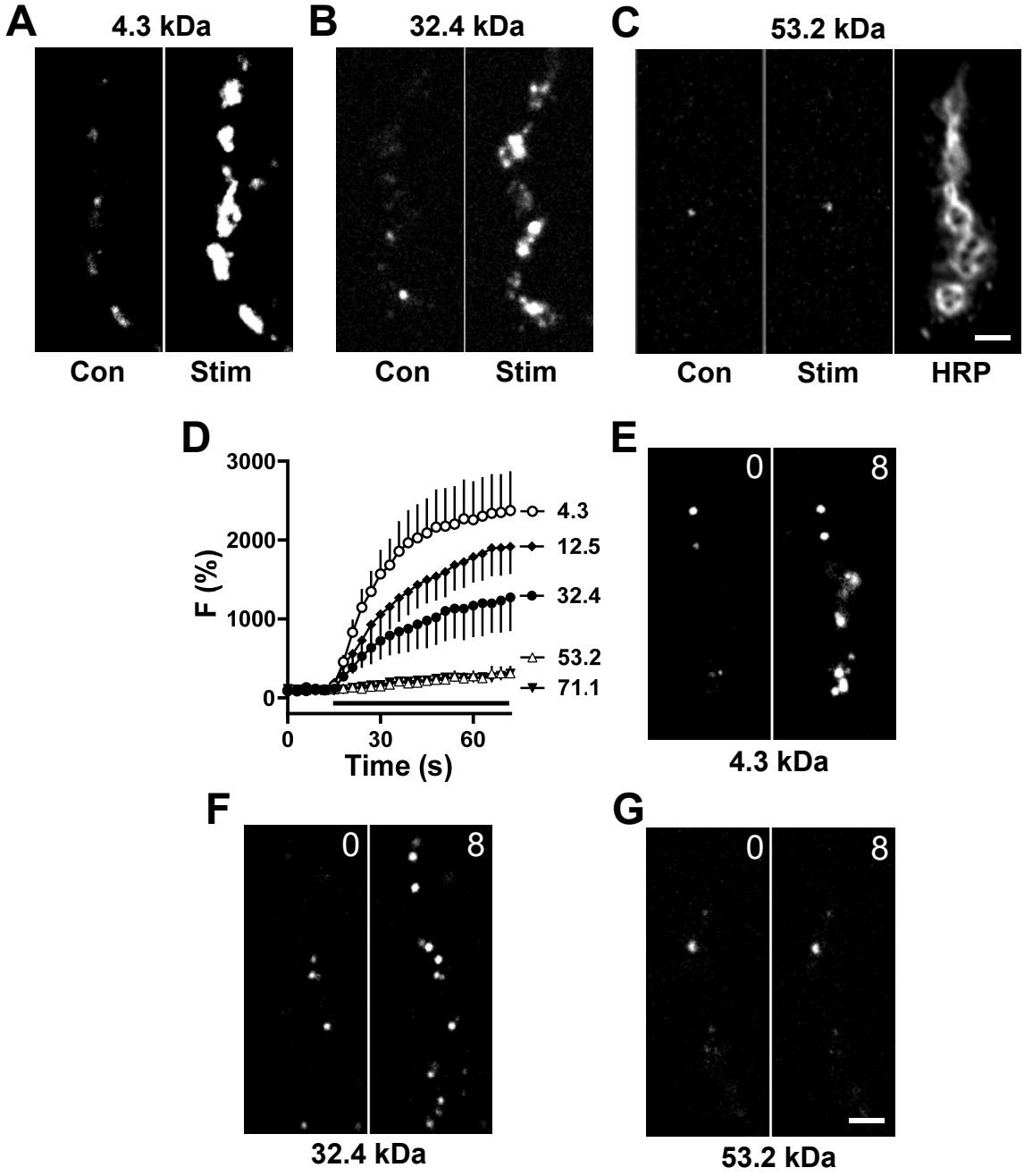

**Figure 2.** Individual spontaneous kiss and run and full fusion events.

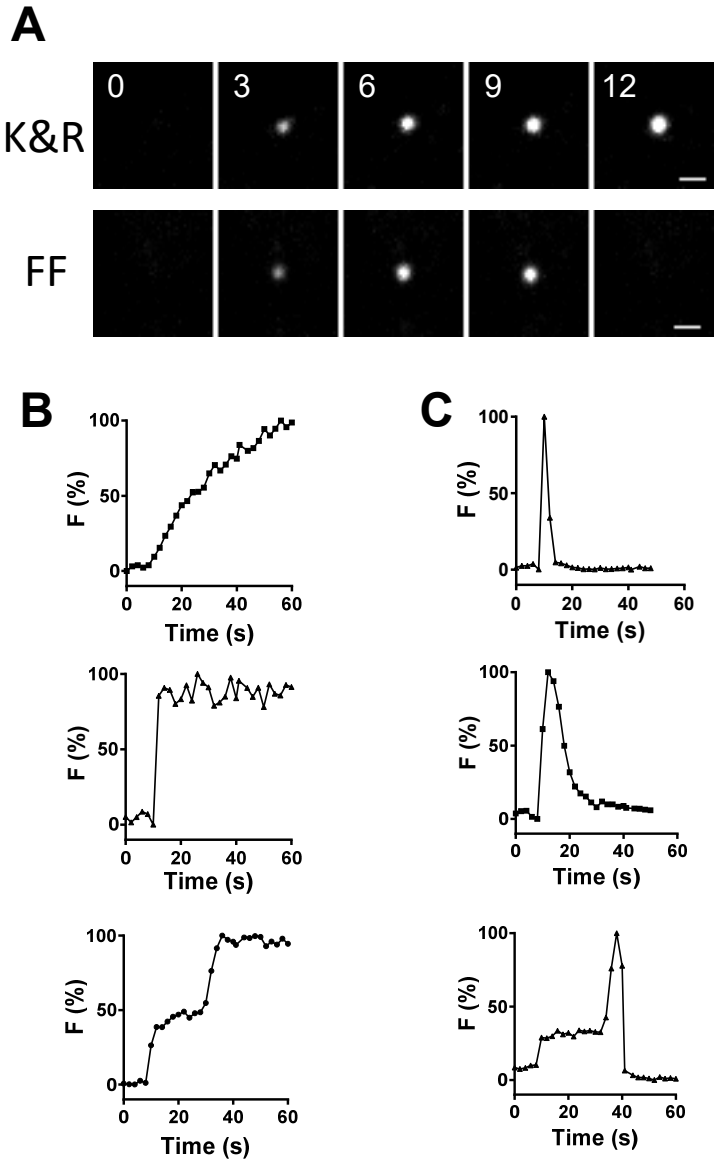

**Figure 3.** cAMP increases the frequency of spontaneous full fusions.

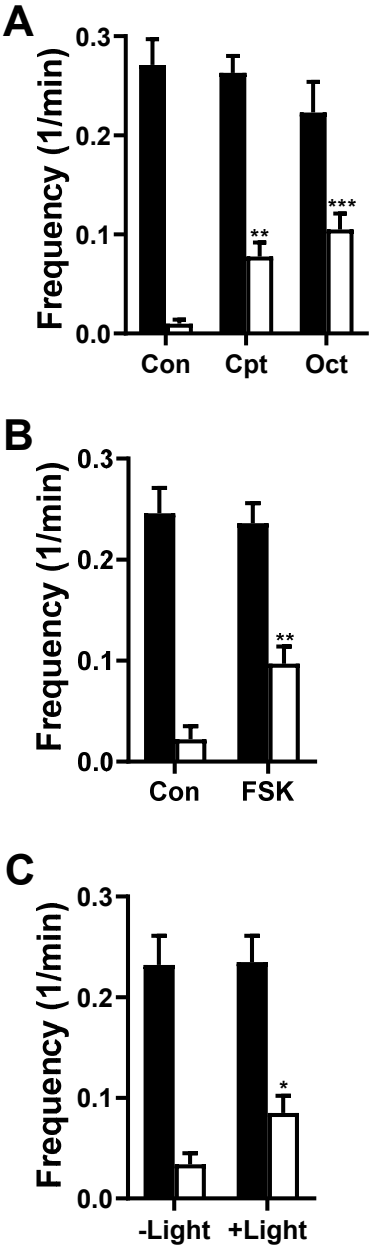

**Figure 4.** Epac is not involved in cAMP-induced full fusions.

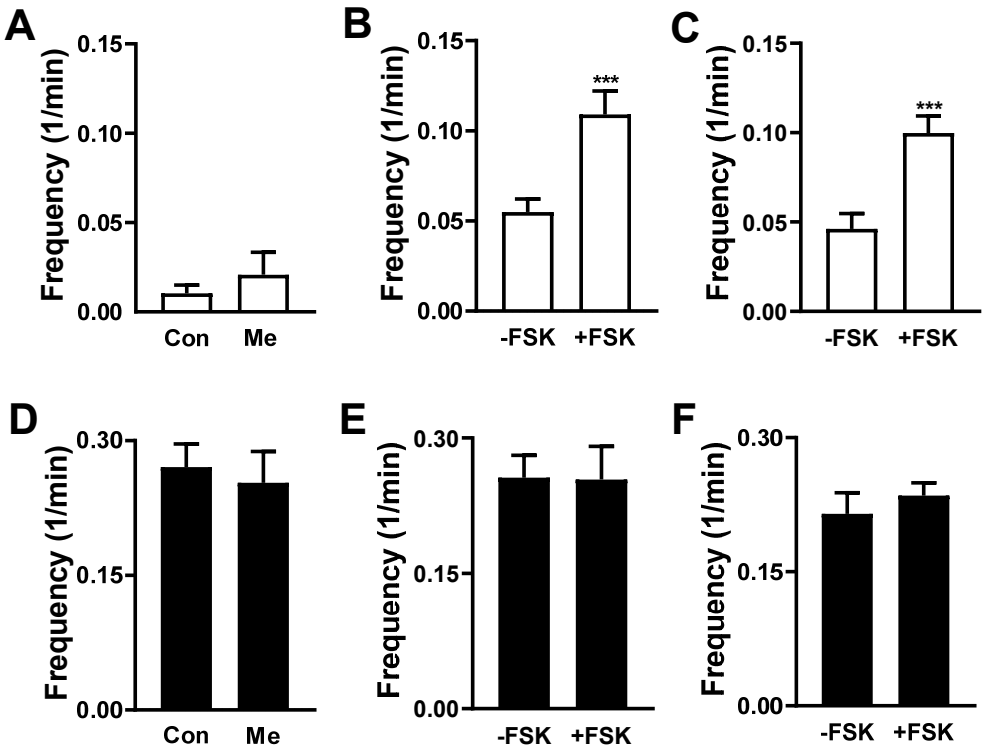

**Figure 5.** cAMP-induced full fusions require anchored PKA-R2.

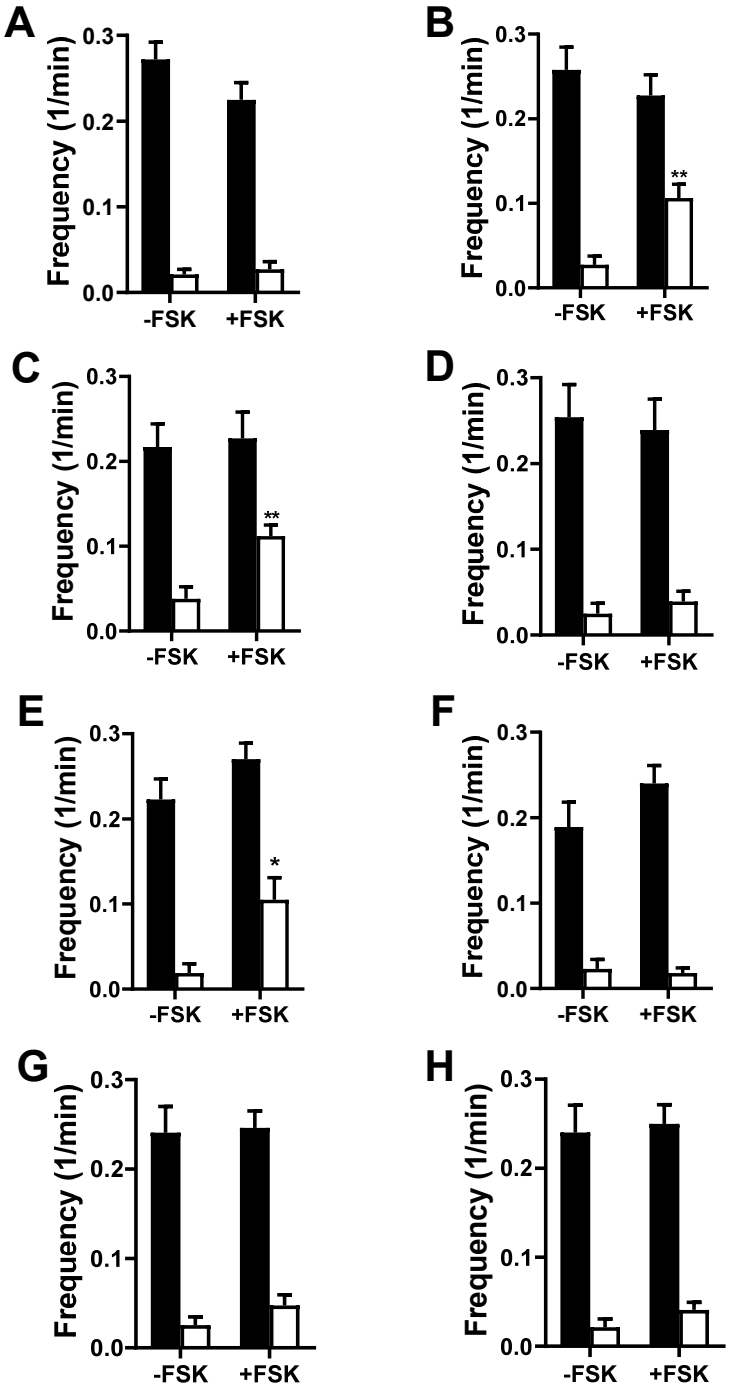
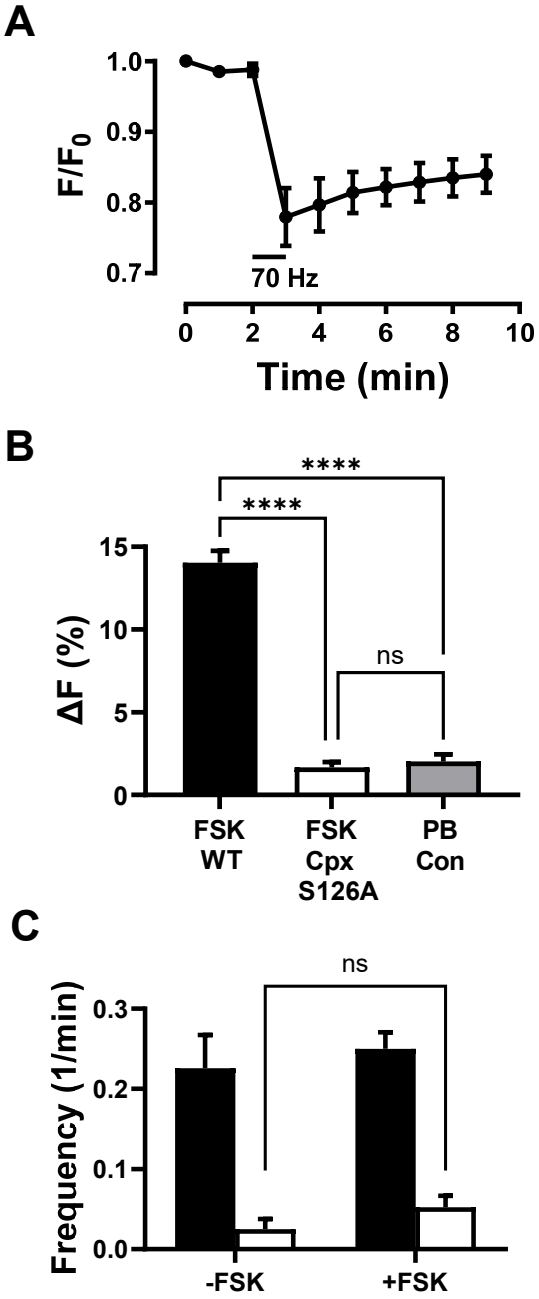
**Figure 6.** The complexin S126 PKA phosphorylation site is required for cAMP-evoked full fusions and neuropeptide release.